Supporting Information

Understanding the structure of isolated iridium sites anchored on a covalent triazine framework

Nina M. Sackers,[†] Andree Iemhoff,[†] Philippe Sautet[‡&] and Regina Palkovits[†]*

[†]Chair of Heterogeneous Catalysis and Technical Chemistry, RWTH Aachen University, Worringerweg 2, 52074 Aachen, Germany

[‡]Department of Chemical and Biomolecular Engineering, University of California, Los Angeles, Los Angeles, California 90095, United States

[&]Department of Chemistry and Biochemistry, University of California, Los Angeles, Los Angeles, California 90095, United States

*Corresponding author: Palkovits@itmc.rwth-aachen.de

Table of Contents

1. Computational Details

All DFT calculations were carried out in a periodic framework using the VASP program series (revision 5.4.4)[1, 2] combined with the PBE exchange-correlation functional[3] within the generalized-gradient approximation (GGA) complemented by Grimme's D3 correction with BJ damping to describe dispersion interactions.[4, 5] The electron-ion interactions were described by the projector-augmented wave method.[6, 7] In order to ensure accurate energies, the energy cut-off of the plane wave basis was set to 400 eV.

Pristine CTF-1 was optimized in a hexagonal unit cell consisting of two CTF layers with the cell parameters a = b = 14.54 Å and c = 6.34 – 7.44 Å depending on the preferred layer distance. The Brillouin zone was sampled by a Γ-centered 3 x 3 x 3 Monkhorst-Pack grid[8] together with a Gaussian smearing of 0.05 eV. A CTF slab was modeled by a double layer in the same cell as pristine CTF but with c = 15.72 Å. At a CTF layer distance of about 3.72 Å, this leads to a vacuum layer of about 12 Å to avoid interactions between the slabs. For geometry optimizations, all atoms were allowed to relax except for one C atom from each CTF layer at the greatest possible distances to the Ir position in the a and b direction to maintain the AA stacking of the CTF. The Brillouin zone was sampled by a Γ-centered 3 x 3 x 1 Monkhorst-Pack grid[8] together with a Gaussian smearing of 0.05 eV. To derive the Bader charges a denser *k*-point mesh of 15 x 15 x 1 was applied, while the (P)DOS was calculated using a 25 x 25 x 1 grid. Calculations of molecular species were conducted in orthorhombic cells of sufficient size to avoid intermolecular interactions (e.g. a = 11 Å, b = 12 Å, c = 14 Å) using the Γ point only. Geometry optimizations of local minima on the potential energy surface were performed with convergence criteria for the electronic self-consistent energy and the ionic relaxation of 10^{-6} eV and 0.02 eV $Å^{-1}$, respectively. The TSs of minimum energy paths were localized by employing the climbing image nudged elastic band (CI-NEB) method[9, 10] with eight movable images between the fixed initial and final stationary points. Every TS was optimized with the improved dimer method[11] using a smaller convergence criterion for ionic relaxation of 0.01 eV $Å^{-1}$. Frequency calculations verified that every localized TS exhibits exactly one imaginary frequency corresponding to the investigated reaction step. For electronic structure analysis, Bader charges were obtained performing the Bader charge analysis by Henkelman.[12] The (P)DOS was extracted from VASP using VASPKIT.[13]

The zero-point energy and thermal contributions to the electronic energy were computed from frequency calculations of the free molecules and all adsorbates using statistical thermodynamics (see Chapter 1.1)[14] at atmospheric pressure and the following temperatures to reflect the

experimental conditions[15]: at 60 °C for the adsorption studies of Ir(acac), at 400 °C for the reduction with H_2 and at 160 °C for modeling in connection with the FADH reaction. Thermal contributions of adsorbed molecules and atoms were calculated according to the harmonic limit. Low-frequency modes of adsorbed systems below 100 cm^{-1} were shifted to 100 cm^{-1} for the calculation of the vibrational entropy and enthalpy.

Adsorption energies G_{ads} were calculated using Eq. 1, where G denotes the Gibbs energy of the isolated adsorbate (A), the catalyst (cat) or the adsorbed system (A/cat).

$$G_{ads} = G_{A/cat} - (G_A + G_{cat}) \quad (1)$$

The activation barrier of the multistep reaction sequence is determined according to the ES model by Kozuch and Shaik.[16] Using the ES approximation, the TOF is calculated according to Eq. 2.

$$\mathrm{TOF} = \frac{k_B \cdot T}{h} \cdot e^{-\frac{ES}{R \cdot T}} \quad (2)$$

1.1. Thermochemistry Calculations

Gibbs free energy

$$G(T) = H(T) - T \cdot S(T)$$

Gibbs free energy of free/solvated gas molecules

$$G(T, p) = (E_{elec} + E_{ZPE} + [H(T) - H(0)]_{vib} + [H(T) - H(0)]_{rot} + [H(T) - H(0)]_{trans}) - T \cdot (S_{trans}(T) + S_{elec}(T) - k \cdot \ln\frac{p}{p_0})$$

Gibbs free energy of adsorbed molecules/atoms

$$G(T, p) = (E_{elec} + E_{ZPE} + [H(T) - H(0)]_{vib}) - T \cdot S_{vib}(T)$$

Enthalpy contributions

$$E_{\mathrm{ZPE}} = \frac{1}{2}\sum_i \nu_i$$

$$[H(T) - H(0)]_{\mathrm{vib}} = kT\sum_i \frac{h \cdot \nu_i}{k \cdot T} \cdot \frac{e^{-\frac{h \cdot \nu_i}{k \cdot T}}}{\left(1 - e^{-\frac{h \cdot \nu_i}{k \cdot T}}\right)}$$

$$[H(T) - H(0)]_{\mathrm{rot}} = \frac{3}{2}kT\,(\text{non - linear}) \text{ or } kT\,(\text{linear})$$

$$[H(T) - H(0)]_{\mathrm{trans}}) = \frac{5}{2}kT$$

Entropy contributions

$$S_{\mathrm{vib}}(T) = \; -k\sum_i \ln\left(1 - e^{-\frac{h \cdot \nu_i}{k \cdot T}}\right) + k\sum_i \frac{h \cdot \nu_i}{k \cdot T} \cdot \frac{e^{-\frac{h \cdot \nu_i}{k \cdot T}}}{\left(1 - e^{-\frac{h \cdot \nu_i}{k \cdot T}}\right)}$$

$$S_{\mathrm{rot}}(T) = k\left[\frac{3}{2}\ln\left(\frac{kT}{h}\right) - \frac{1}{2}\ln\left(\frac{\mathrm{ABC}}{\pi}\right) - \ln\sigma + \frac{3}{2}\right](\text{non - linear}) \text{ or } k\left[\ln\left(\frac{kT}{\sigma hB}\right) + 1\right]\,(\text{linear})$$

$$S_{\mathrm{trans}}\,(T) = \; k\left[\frac{3}{2}\ln\left(\frac{2\pi m}{h^2}\right) + \frac{5}{2}\ln\,(kT) + \frac{5}{2}\right]$$

$$S_{\mathrm{elec}}(T) = k \cdot \ln\,(2 \cdot (\text{total spin}) + 1)$$

2. Modelling of CTF-1

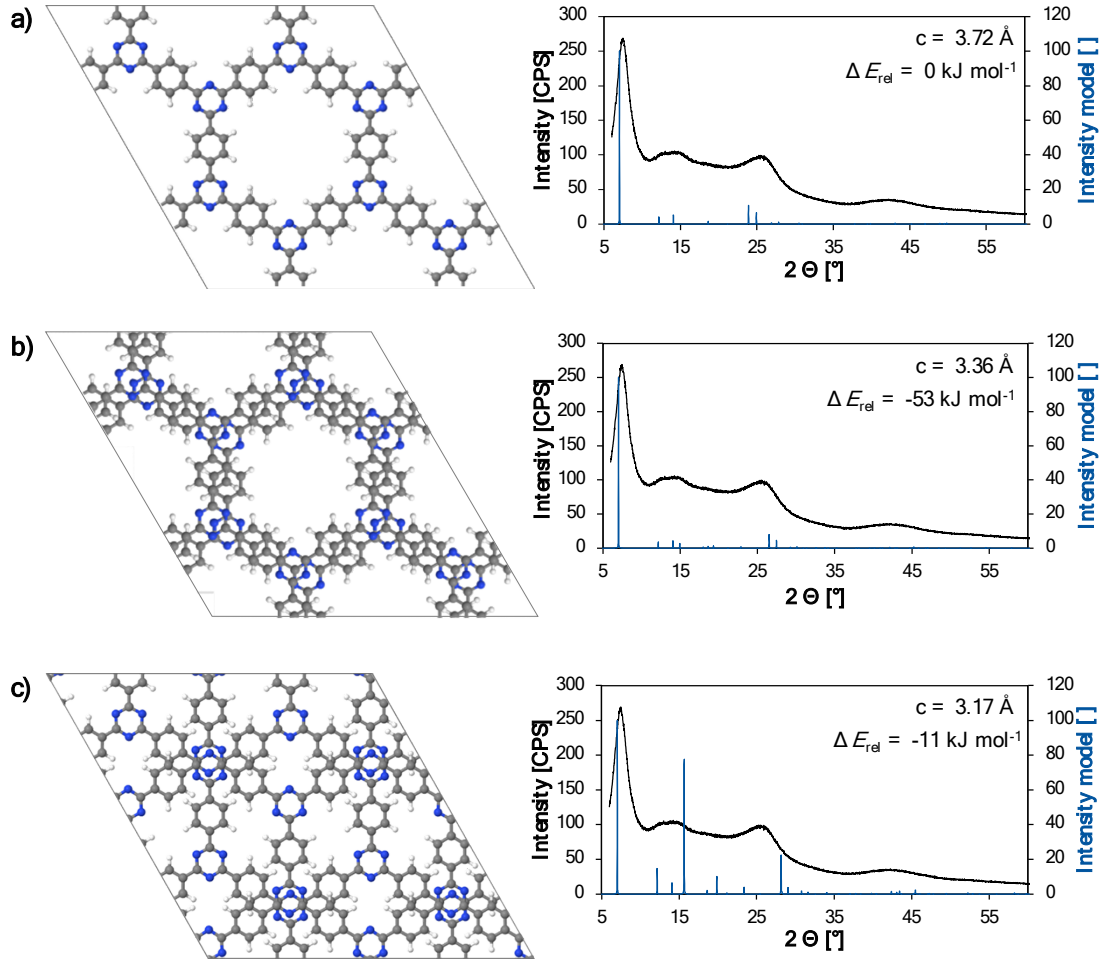

Figure S1. 2x2 supercells of CTF with a) perfect AA, b) shifted AA and c) AB stacking as well as corresponding simulated XRD data compared to the experimental results from Iemhoff et al.[15]

Table S1. Experimental and computational cell parameters of pristine CTF.

Cell parameter	Literature value[a]	Computational model with perfect AA stacking[b]	Computational model with shifted AA stacking[b]
a = b [Å]	14.48	14.54 (+ 0.4%)	14.54 (+ 0.4%)
c [Å]	3.62	3.72 (+ 2.7%)	3.36 (- 7.2%)

[a] Determined via Pawley refinement from XRD data.[17]
[b] Values in brackets indicate the deviation from literature values.

3. Ir(acac)/CTF as Synthesized

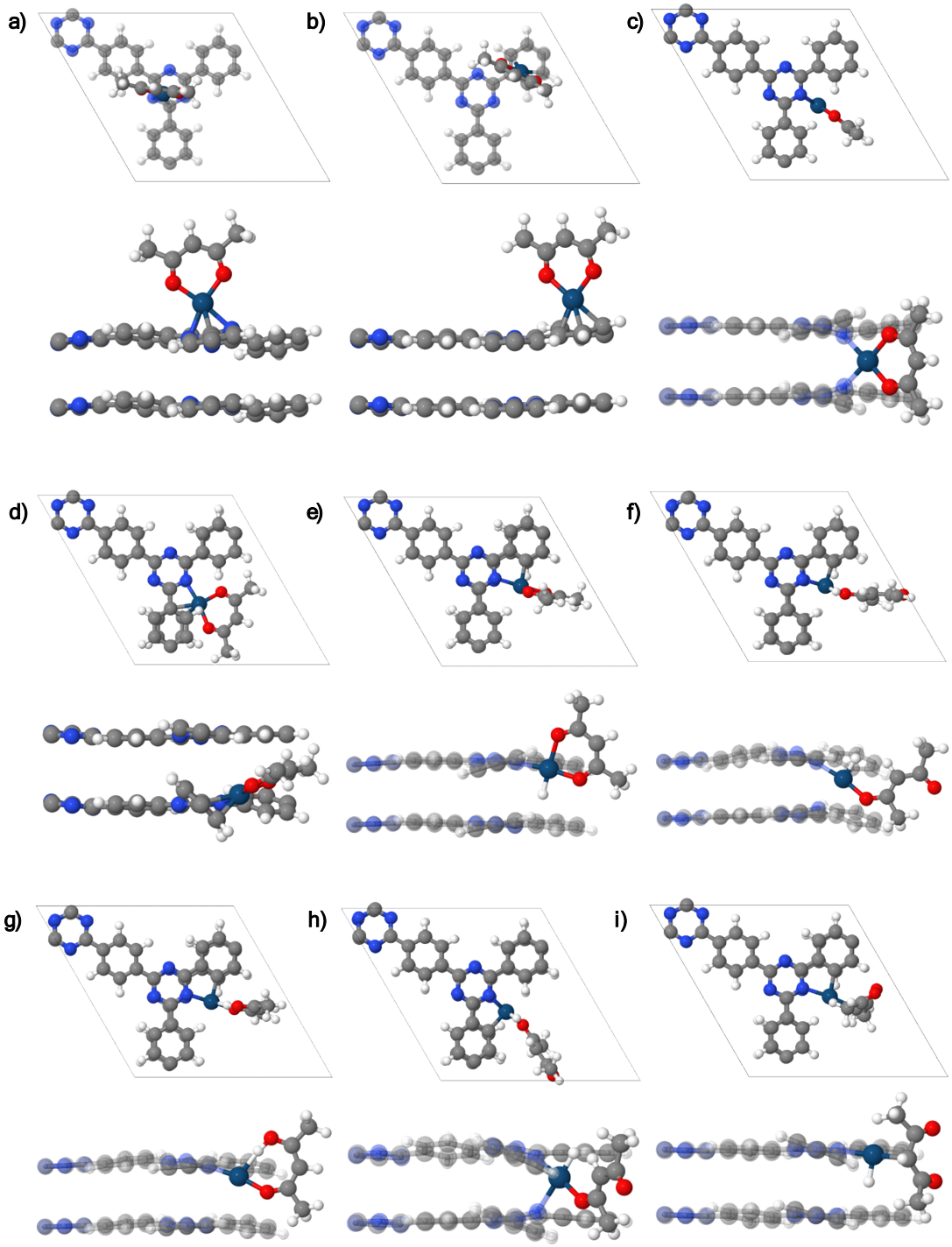

Figure S2. Potential adsorption geometries for Ir(acac) on CTF-1: a-b) on top of the CTF, c-d) between two CTF layers, e-i) with C-H activation of the phenyl.

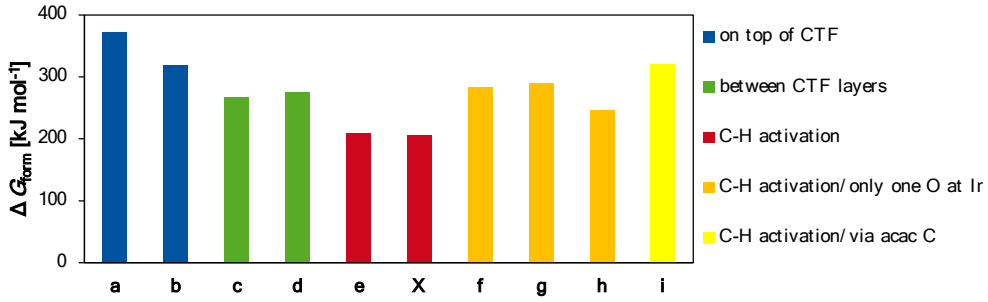

Figure S3. Formation Gibbs energies of Ir(acac) immobilized on CTF referenced to Ir(acac)(COD) at 60 °C. X denotes the most stable geometry depicted in Figure 2.

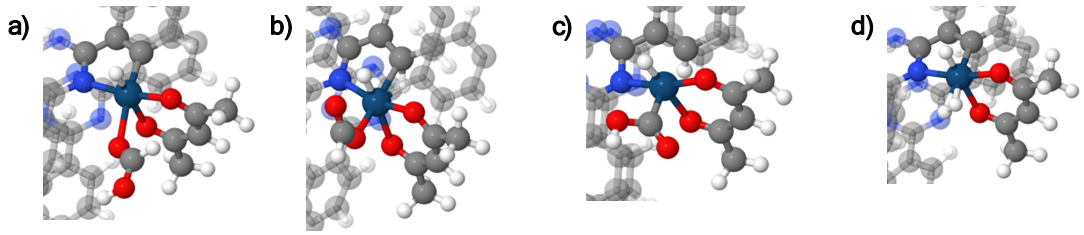

Figure S4. Adsorption of a) FA, b) formate and H, c) carboxyl and H and d) H_2 on the most stable Ir(acac)/CTF geometry.

Table S2. Adsorption Gibbs energies of reactant, potential intermediates and product of the FADH at Ir(acac)/CTF at 160 °C.

Adsorbate	ΔG_{ads} [kJ mol^{-1}]
HC(O*)OH	194
H* + (C*)OOH	161
H* + HCOO*	278
H*-H*	144

Table S3. Adsorption Gibbs energies of reactant, potential intermediates and product of the FADH on various Ir(acac)/CTF models at 160 °C.

Catalyst model from Figure S2	Adsorbate	ΔG_{ads} [kJ mol^{-1}]
c	H* + HCOO*	248
	H* + (C*)OOH	294
e	HC(O*)OH	169
	H* + HCOO*	244
	H* + (C*)OOH	177
	H*-H*	102
f	HC(O*)OH	177
	H* + HCOO*	242
	H* + (C*)OOH	241
	H*-H*	119
h	HC(O*)OH	230
	H* + HCOO*	206
	H* + (C*)OOH	167
	H* + H*	88
	OCO*	199
f/1[a]	HC(O*)OH	254
	H* + HCOO*	163
	H* + (C*)OOH	244
	H*-H*	148
f/2[b]	HC(O*)OH	233
	H* + HCOO*	183
	H* + (C*)OOH	244
	H*-H*	147

[a] H from Ir-H bond shifted to form acetylacetone instead of acac.
[b] H from Ir-H bond shifted to form enol form of acetylacetone instead of acac.

4. Ir/CTF after Reduction at 400 °C

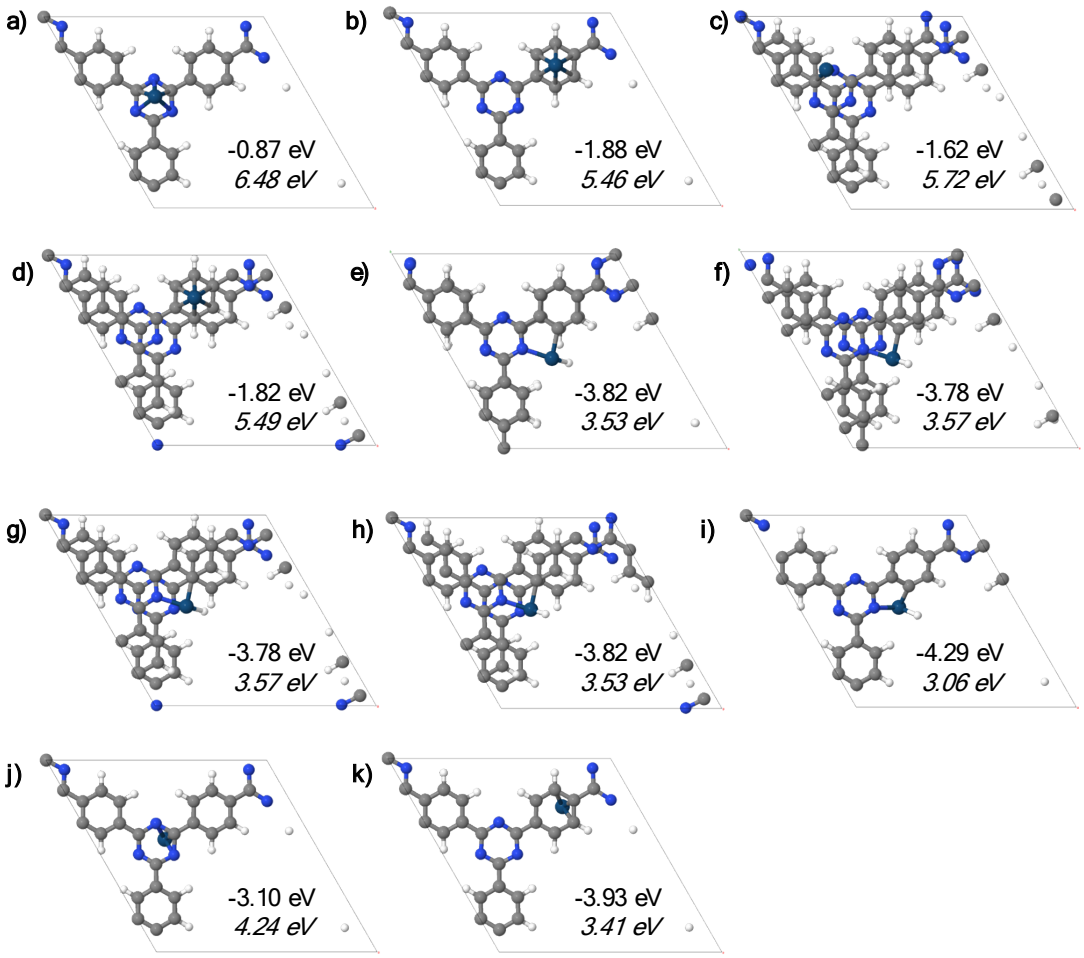

Figure S5. Potential positions of Ir for an interaction with CTF-1. a-d) on top of CTF, e-h) with one C-H activation of the CTF, i) with two C-H activations of the CTF, j-k) between the CTF layers. Non-italic: Energy of formation from Ir gas and CTF, italic: Stability against agglomeration of Ir.

Figure S6. Front and side view of the benchmark Ir/CTF structure from Figure S5 i.

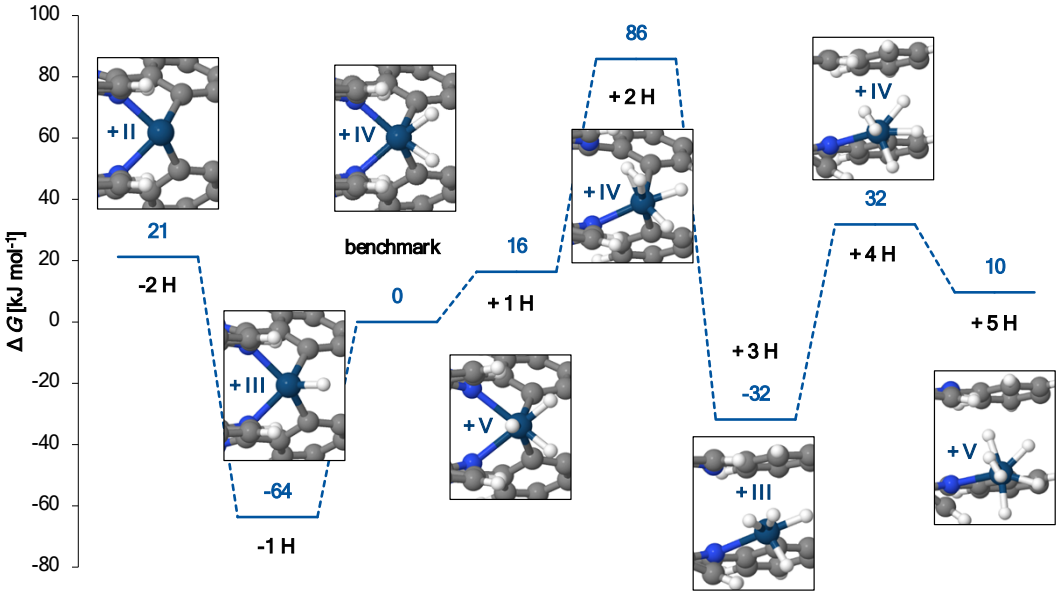

Figure S7. Hydrogenation stages of the Ir atom in Ir/CTF referenced to H2 in the gas phase at 400 °C and atmospheric pressure. Formal oxidation states are denoted in roman numbers.

Table S4. Results of the EXAFS fit of the Ir/CTF reduced at 400 °C by Iemhoff et al.[15]

Quantity	Ir-N/Ir-C_1	Ir-C_2
Coordination number	4	4
R [Å]	2.0364 ± 0.0129	2.9347 ± 0.0313

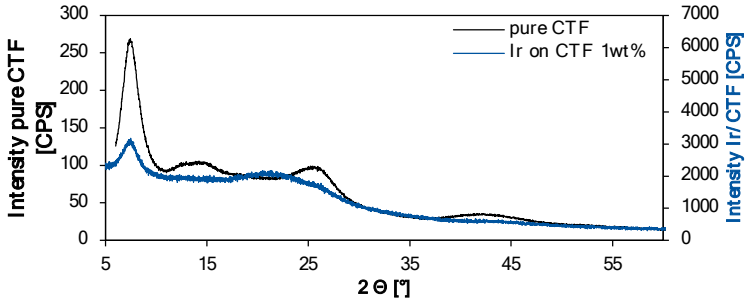

Figure S8. XRD spectra of pure CTF as well as Ir/CTF after reduction in H_2 at 400 °C with 1 *wt.*% Ir.

Table S5. Bader charges at selected atoms of Ir catalysts on CTF as well as their precursor compounds.

Material	*q*(Ir) [|e|]	*q*(H) [|e|]	*q*(C_{up}) [|e|]	*q*(C_{low}) [|e|]	*q*(N_{up}) [|e|]	*q*(N_{low}) [|e|]
Ir/CTF	+0.61	-0.03	-0.10	-0.07	-1.16	-1.14
Ir(acac)/CTF	+0.85	-0.11	0.00	+0.02	-1.11	-1.19
CTF	-	+0.10	-0.08	-0.08	-1.19	-1.19
Ir(acac)(COD)	+0.69	-	-	-	-	-

Charges of the atoms coordinating Ir in Ir/CTF. up/low indicate the upper/lower CTF layers.

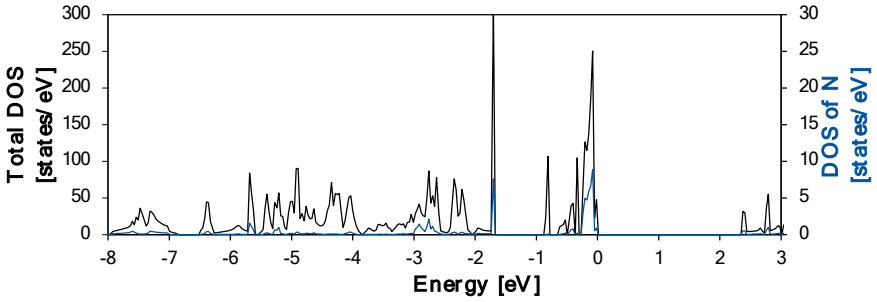

Figure S9. Total DOS and DOS of N from pristine CTF.

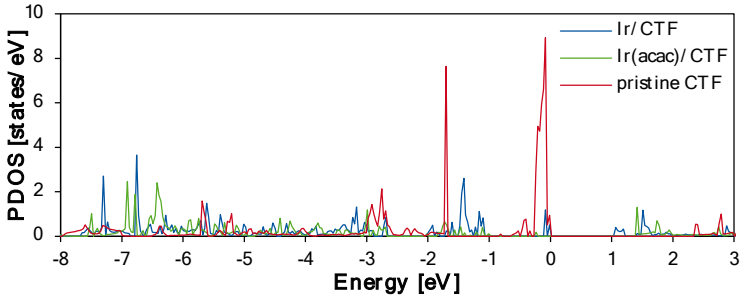

Figure S10. PDOS of N in Ir/CTF, Ir(acac)/CTF and pristine CTF.

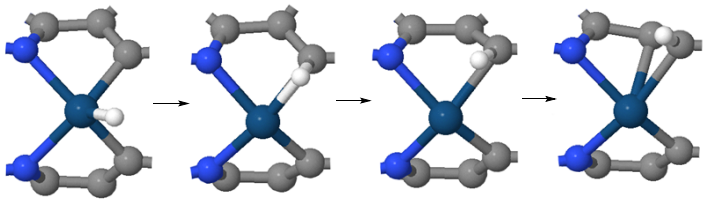

Figure S11. Local minima of the migration of H from Ir to the phenyl C in Ir/CTF.

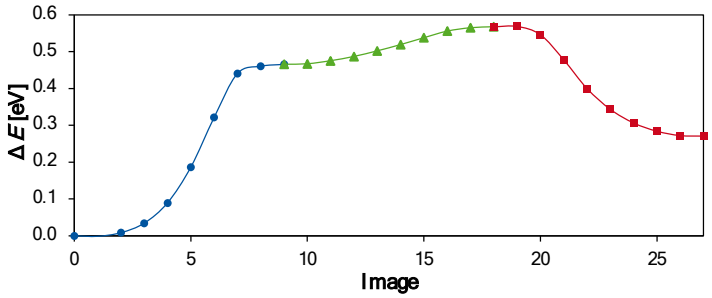

Figure S12. CI-NEB for the C-H recovery in the most stable Ir/CTF structure.

Figure S13. Energy profile of the FADH on Ir/CTF following the formate pathway.

Figure S14. Energy profile of the FADH on Ir/CTF following the carboxyl pathway. *TS connecting these minima was not localized but is not considered having an influence on the overall activation barrier.

5. References

1 G. Kresse and J. Hafner, *Phys. Rev. B*, 1994, **49**, 14251.

2 G. Kresse and J. Furthmüller, *Comput. Mater. Sci.*, 1996, **6**, 15-50.

3 J. P. Perdew, K. Burke and M. Ernzerhof, *Phys. Rev. Lett.*, 1996, **77**, 3865.

4 S. Grimme, J. Antony, S. Ehrlich and H. Krieg, *J. Chem. Phys.*, 2010, **132**, 154104.

5 S. Grimme, S. Ehrlich and L. Goerigk, *J. Comput. Chem.*, 2011, **32**, 1456-1465.

6 P. E. Blöchl, *Phys. Rev. B*, 1994, **50**, 17953.

7 G. Kresse and D. Joubert, *Phys. Rev. B*, 1999, **59**, 1758.

8 H. J. Monkhorst and J. D. Pack, *Phys. Rev. B*, 1976, **13**, 5188.

9 G. Henkelman, B. P. Uberuaga and H. Jónsson, *J. Chem. Phys.*, 2000, **113**, 9901-9904.

10 G. Henkelman and H. Jónsson, *J. Chem. Phys.*, 2000, **113**, 9978-9985.

11 G. Henkelman and H. Jónsson, *J. Chem. Phys.*, 1999, **111**, 7010-7022.

12 G. Henkelman, A. Arnaldsson and H. Jónsson, *Comput. Mater. Sci.*, 2006, **36**, 354-360.

13 V. Wang, N. Xu, J.-C. Liu, G. Tang and W.-T. Geng, *Comput. Phys. Commun.*, 2021, **267**, 108033.

14 K. K. Irikura and D. J. Frurip, in *Computational Thermochemistry*, American Chemical Society, 1998, ch. 22, pp. 402-418.

15 A. Iemhoff, M. Vennewald, J. Artz, C. Mebrahtu, A. Meledin, T. E. Weirich, H. Hartmann, A. Besmehn, M. Aramini and F. Venturini, *ChemCatChem*, 2022, **14**, e202200179.

16 S. Kozuch and S. Shaik, *Acc. Chem. Res.*, 2011, **44**, 101-110.

17 M. Liu, K. Jiang, X. Ding, S. Wang, C. Zhang, J. Liu, Z. Zhan, G. Cheng, B. Li and H. Chen, *Adv. Mater.*, 2019, **31**, 1807865.